
**Liquid Crystals**
Publication details, including instructions for authors and subscription information:
http://www.informaworld.com/smpp/title~content=t713926090

# Landau-de Gennes theory of the core structure of a screw dislocation in smectic A liquid crystals

S. Kralj[ab]; T. J. Sluckin[a]
[a] Faculty of Mathematical Studies, University of Southampton, Southampton, England [b] Institute Jozef Stefan, Ljubljana, Slovenia

**To cite this Article** Kralj, S. and Sluckin, T. J.(1995) 'Landau-de Gennes theory of the core structure of a screw dislocation in smectic A liquid crystals', Liquid Crystals, 18: 6, 887 — 902
**To link to this Article: DOI:** 10.1080/02678299508036707
**URL:** http://dx.doi.org/10.1080/02678299508036707

LIQUID CRYSTALS, 1995, VOL. 18, NO. 6, 887–902

# Landau–de Gennes theory of the core structure of a screw dislocation in smectic A liquid crystals

by S. KRALJ*† and T. J. SLUCKIN
Faculty of Mathematical Studies, University of Southampton, Southampton SO17 1BJ, England

*(Received 9 February 1994; in final form 26 September 1994; accepted 10 November 1994)*

We present details of calculations of the core structure of a screw dislocation in a smectic A liquid crystal, using the phenomenological Landau–de Gennes free energy functional. The order parameter frustration created by topological constraints far from the dislocation core is resolved in one of three qualitatively different ways. The three types of dislocation core solution are the DT (double twist), CL (classical), and BP (broken polar symmetry) solutions, respectively. The stability requirements for these structures are discussed, as a function of temperature, smectic elastic properties, and coupling between smectic and nematic order. The effect of possible inhomogeneity between left- and right-handed conformers is also examined.



## 1. Introduction

The study of defects in solid and liquid state physics made major progress when it was realized that a coherent classification of such defects could be made using homotopic ideas borrowed from topology [1, 2]. Nevertheless, it is clear that although topological constraints have a major influence on defect dynamics and even statics in condensed matter systems, there remains interesting physics on smaller length scales, which is not completely determined by these topological conditions. In this paper, we discuss one such problem: the core of a screw dislocation in a smectic A liquid crystal.

We set the scene for this study by pointing out that liquid crystals are particularly appropriate vehicles for the study of defects. Their fluidity allows the physical relaxation implicit in topological discussions. The mesoscopic nature of liquid crystals provides a wealth of order parameters which provide the basic preconditions for defected physical systems. The equilibrium order parameter manifold is often embedded in a higher order manifold. This permits a 'microscopic' topology differing from that defined by the hydrodynamic scale, and thus introduces naturally a microscopic classification of defect structure [3]. Unlike in many solids, there is also the possibility of a decoupling between orientational and translational degrees of freedom.

It is helpful to recall some of the salient relevant features of the smectic A ($S_A$) liquid crystalline phase in equilibrium [4]. It may be regarded as consisting of a stack of parallel two-dimensional nematic (N) layers; the average distance between layers is comparable to the molecular length. Within each layer there is no translational order. The nematic director $\mathbf{n}(\mathbf{r})$ is parallel to the layer normal, and thus strongly resists the twist and bend deformations which occur in nematic hydrodynamics. Mathematically the absence of twist and bend is equivalent to the statement that the layer thickness is constant, or equivalently $\nabla \times \mathbf{n} = 0$.

The layered $S_A$ structure is commonly represented by a complex density wave $\psi(\mathbf{r})$. de Gennes [5] was the first to point out that the free energy functional constructed from the symmetry-allowed combination of order parameters closely resembles the Landau–Ginzburg hamiltonian used to discuss the normal state-super conductor transformation in low temperature metals. In this analogy, the smectic order parameter $\psi$ plays the role of the Cooper-pair density and the nematic director field $\mathbf{n}$ plays the role of the magnetic vector potential $\mathbf{A}$. This has particular relevance, because a superconductor placed in a magnetic field $\mathbf{B} = \nabla \times \mathbf{A}$ may go through a type *I*–type *II* transformation, in which a lattice of line defects in the Cooper pair density vortices–is created. Only within the vortices can the magnetic field $\mathbf{B}$ penetrate. This lattice is often known as the Abrikosov lattice and the phase as the Abrikosov phase [6].

Renn and Lubensky [7, 8] realized that the $S_A$ superconductor analogy was also relevant in this context. The $S_A$ analogue of the magnetic field $\mathbf{B}$ is the de Gennes molecular field $\mathbf{h} = \nabla \times \mathbf{n}$. This quantity is non-zero in a chiral nematic (N*), and there is a term in the free energy coupling to $\mathbf{h}$ even if the N* phase is replaced by $S_A$. Renn and Lubensky realized that there was an $S_A$ analogy to the

* Author for correspondence.
† Permanent address*: Institute Jozef Stefan, Jamova 39, Ljubljana 61000, Slovenia.

0267–8292/95 $10-00 

Abrikosov phase, in which now the twist (i.e. regions in which $\nabla \times \mathbf{n} \neq 0$) is confined to a lattice of screw dislocations.

This is the twist grain boundary (TGB), or $S_A^*$ phase. It consists of a regular array of parallel 'twist grain' boundaries, each of which is made up of a set of regularly spaced parallel screw dislocations. Between the grain boundaries the molecular configuration is essentially identical to that in the non-chiral $S_A$ phase. The screw dislocation axes rotate from one grain boundary to the next in a helical fashion. In this way it is possible for smectic layering and spontaneous chiral-induced nematic twist to coexist. Recent experiments support this picture [9, 10].

The basic building block of the TGB phase, however, is the screw dislocation, and this remains incompletely understood. Day *et al.* [11], used the analogy between the $S_A$ phase and superconductors. They show that the director field close to the dislocation axis can be obtained by directly mapping the magnetic vortex problem onto the $S_A$ problem. Their results are valid in the continuum limit. Loginov and Terentjev [12] have also studied screw dislocation core structure. They draw an analogy with dislocations in solids [13] and obtain the core structure in a continuum-like approximation in which $\mathbf{n}$ is constrained to be everywhere locally perpendicular to the layers.

Each of these approximations has a range of validity. Nevertheless, it is important to take account of the possibility, not only of varying $\mathbf{n}$, but also of varying nematic and smectic order parameters in the dislocation region. The purpose of this paper is to show that, in fact, the structure of the screw dislocation core in the $S_A$ phase can be considerably more complex than its analogue in the theory of superconductivity. We minimize the de Gennes free energy functional; this takes into account, in a covariant way, variations in the nematic and smectic order parameters.

The paper is organized as follows. In § 2 we present the model free energy density and corresponding bulk phase diagram. In § 3 we derive three qualitatively different screw dislocation core structures, and in § 4 discuss their stability. In § 5 we examine the case in which the nematic phase is composed of a mixture of conformers with opposite molecular chirality. This affects both the order parameter structure and the conformer concentration profile in the dislocation region. Finally in § 6 we present a brief discussion of our results. Some technical details have been relegated to the appendices.

A preliminary account of these results has already been presented [14].

## 2. Model

### 2.1. *Free energy*

A screw dislocation is but one example of an inhomogeneous structure embedded in a $S_A$ system. In our approach, an inhomogeneity is completely described by (i) the complex order parameter $\psi(\mathbf{r})$; (ii) the nematic director field $\mathbf{n}(\mathbf{r})$; (iii) the nematic orientational order parameter $S(\mathbf{r})$. In principle one could imagine more complicated descriptions which would take into account, for example, different Fourier harmonics of the density $\rho(\mathbf{r})$, or biaxiality in the (tensor) nematic order parameter $S(\mathbf{r})$. Our choice of relevant order parameters (apart from being conventional) is the minimal set which allows sensible discussion of defect structure in smectics [15].

The quantity $\psi(\mathbf{r})$ models the layered structure of the $S_A$ phase. It is related to the first harmonic of the density deviation $\delta\rho(\mathbf{r})$ from a homogeneous distribution. In a uniform smectic

$$\psi(\mathbf{r}) = \eta(\mathbf{r}) \exp(i\mathbf{q}\cdot\mathbf{r}) = \eta(\mathbf{r}) \exp[i\phi(\mathbf{r})].$$

The degree of layer ordering is measured by the scalar order parameter $\eta$; the phase $\phi$ determines the smectic layer position; $\mathbf{q} = 2\pi/d_0\mathbf{n}$ and $d_0$ is the equilibrium layer spacing.

The free energy density $f(\mathbf{r})$ is expressed in terms of the relevant order parameters as the sum of nematic (N) and smectic (S) local and non-local terms

$$f(\mathbf{r}) = f_N^{loc} + f_N^{non} + f_S^{loc} + f_s^{non} f_{coupl}, \tag{1}$$

$$f_N^{loc} = a_0 \frac{(T - T_{NI}^*)}{T_{NI}^*} \frac{S^2}{2} - b\frac{S^2}{3} + c\frac{S^4}{4}, \tag{1a}$$

$$f_N^{non} = \tfrac{1}{6}(k_\parallel(\mathbf{n}\cdot\nabla S)^2 + k_\perp(\mathbf{n}\times\nabla S)^2) + S^2\left(\frac{k_1}{2}(\nabla\cdot\mathbf{n})^2 + \frac{k_2}{2}(\mathbf{n}\cdot\nabla\times\mathbf{n})^2 + \frac{k_3}{2}(\mathbf{n}\times\nabla\times\mathbf{n})^2\right), \tag{1b}$$

$$f_S^{loc} = \alpha_0 \frac{(\mathbf{T} - T_{SN}^*)}{T_{SN}^*}|\psi|^2 + \frac{\beta}{2}|\psi|^4 + \frac{\gamma}{3}|\psi|^6, \tag{1c}$$

$$f_S^{non} = \gamma_\parallel|(\mathbf{n}\cdot\nabla - iq_0)\psi|^2 + \gamma_\perp|\mathbf{n}\times\nabla\psi|^2, \tag{1d}$$

$$f_{coupl} \propto -DS|\psi|^2. \tag{1e}$$

Although this free energy functional has been used elsewhere, it is worth discussing in slightly more detail the physical meaning of the terms therein.

The quantity $f_N^{loc}$ describes the contribution from the nematic order parameter alone, under the assumption of a non-varying uniaxial order parameter. It is the usual Landau–de Gennes order parameter expansion in this context, with phenomenological expansion constants $a_0$, $b$, $c$, $T_{NI}^*$ obtained from experiment.

The quantity $f_N^{non}$ describes contributions from changes in the nematic order. These are of two types: (i) the usual Frank elastic energy contributions, in which the director changes, and (ii) contributions which describe changes in the degree of nematic order. We make the hypothesis that the Frank constants $K_i = k_i S^2$, where $i = 1, 2, 3$ correspond to splay, twist and bend constants, respectively. We also introduce two constants $k_\parallel$ and $k_\perp$, which describe changes in $S(\rho)$, respectively parallel to and perpendicular to the director. These constants influence the orientation of $\mathbf{n}(\mathbf{r})$ at the isotropic–nematic interface. In this free energy expression there are thus five independent elastic constants, and this is what is permitted by symmetry. Of course a more detailed tensor discussion [16, 17] does suggest relationships between these constants; the tensor Landau–de Gennes theory allows only two independent lowest order bulk elastic constants. In the calculations presented in this paper $k_i (i = 1, 2, 3, \perp, \parallel)$ are temperature independent, although this is not an essential feature of the model.

There are similar terms $f_S^{loc}$ and $f_S^{non}$ corresponding to 'pure smectic' contributions. The complex order parameter $\psi(\mathbf{r})$ can only enter at quadratic order. The parameters $\alpha_0, \beta, \gamma, T_{SN}^*$ describe an 'ideal' smectic free energy uninfluenced by the propinquity of a nematic phase. In fact, there is also a coupling term $f_{coupl}$ involving both smectic and nematic order parameters; this term plays an important role in determining the nature of the N–$S_A$ phase transition [4, 18].

All smectic elastic effects are described by the parameters $\gamma_\perp$ and $\gamma_\parallel$ in $f_S^{non}$; the latter is associated with layer compression, and the former measures the cost of tilting the director away from the layer normal. Thus the condition $\gamma_\perp \to 0$ corresponds to an instability of the $S_A$ phase with respect to $S_C$ fluctuations. The layer thickness $d = 2\pi/q_0$ is enforced, at least in ideal systems, by the phase of the complex smectic order parameter $\psi(\mathbf{r})$.

Finally we emphasize that we are using this free energy functional in a purely mean-field context. Lubensky *et al.* [19] have used relevant parts of this functional as a Landau–Ginzburg–Wilson functional in order to describe critical phenomena close to smectic onset in the nematic phase. In particular, this leads to divergences of $K_2$ and $K_3$ at a second order N–$S_A$ transition. However, inside the smectic phase, finite values of $K_2$ and $K_3$ are nevertheless consistent with the non-existence of hydrodynamic twist and bend deformations.

Equations (1) contain a large number of variables. It therefore proves convenient to carry out some scaling transformations. We define scaled nematic and smectic order parameters $s = Sc/b$ and $\varepsilon = \eta\sqrt{(\gamma/b)}$. We measure position in terms of a dimensionless coordinate $\mathbf{x} = q_0\mathbf{r}$. In this language, the layer thickness is just $2\pi$; i.e. phase angle and length in an undistorted system coincide.

We now obtain a dimensionless free energy density

$$g(\mathbf{x}) = g_{bulk} = f(\mathbf{x})\frac{c^3}{b^4} = g_N^{loc} + C_1 g_N^{non} + C_2 g_S^{loc} + C_3 g_S^{non} + g_{coupl}. \quad (2)$$

The detailed structure of the individual terms in $g(\mathbf{x})$ will be given in the next sub-section. The three coupling constants $C_1$, $C_2$, $C_3$ set the relative energy scales for nematic inhomogeneities, smectic bulk order and smectic inhomogeneities as compared to nematic bulk order. The coupling constants are defined by

$$C_1 = k_1 q_0^2 c/b^2;\ C_2 = (\beta c)^3/(\gamma b^2)^2;\ C_3 = \beta c^3 q_0^2 \gamma_\parallel/(\gamma\beta^4). \quad (3)$$

The ratios of these constants reveal characteristic lengths involved in our problem as shown in § 2.3.

### 2.2. *Bulk phase diagram*

All simple theories of the I–N–$S_A$ phase diagram have the following features [20–22]. At low coupling between the nematic and smectic order parameters, the progression of phases with decreasing temperature is I, N, $S_A$: the I–N phase transition is first order (as determined by symmetry considerations), and the $X$–$Y$-like order parameter permits the N = $S_A$ transition to be continuous. As the coupling is increased, the transition temperature $T_{SN}$ increases, and eventually there is a tricritical point, beyond which the transition is first order. As coupling is further increased, $T_{SN}$ increases further until it reaches $T_{NI}$ at a triple point. Beyond this coupling, the nematic phase is pre-empted by a direct isotropic–smectic phase transition at $T_{SI}$. In this section we briefly describe quantitively how this scenario develops within the scope of the Landau–de Gennes model that we consider. This bulk phase diagram is crucial in order to interpret the regions of validity of various dislocation core structures.

In the absence of deformations the dimensionless free energy takes the form

$$g = g_{bulk} = g_N^{loc} + C_2 g_+^{loc} g_{coupl}, \quad (4)$$

where

$$g_N^{loc} = (t - t_n)\frac{s^2}{2} - \frac{s^3}{3} + \frac{s^4}{4}, \quad (4a)$$

$$g_S^{loc} = (rt - t_s)\epsilon^2 + \frac{\epsilon^4}{2} + \frac{\epsilon^6}{3}, \quad (4b)$$

$$g_{coupl} = -Ds\epsilon^2. \quad (4c)$$

In these equations $t = (T/T_{NI})(ca_0/b^2)$ is the scaled temperature,

$$r = \gamma\alpha_0 b^2/(ca_0\beta)^2(T_{NI}^*/T_{SN}^*),\ t_S = \gamma\alpha_0/\beta^2, \text{ and } t_n = ca_0/b^2.$$

In the $D = 0$ weak coupling limit, the N–$S_A$ transition is continuous at $t = t_S/r$, and the I–N transition is

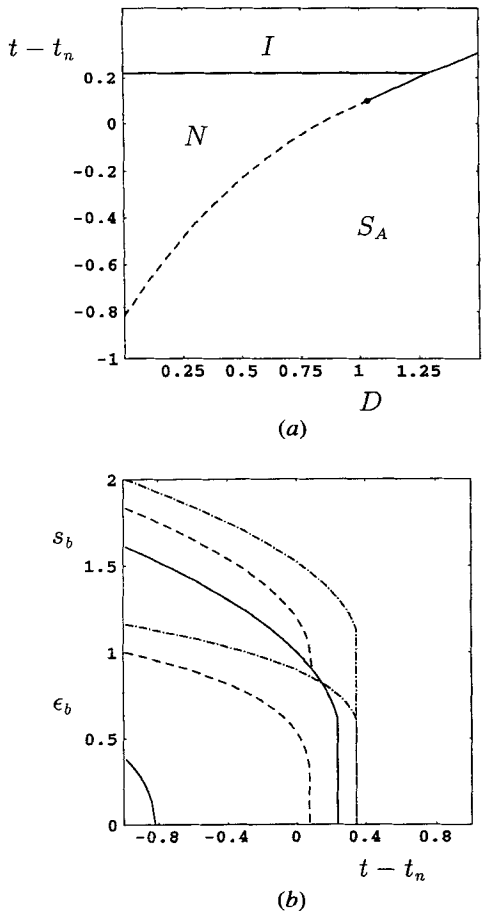


Figure 1. Bulk properties of the model studied for $C_2 = 1$, $t_n = t_S = 50$, $r = 1{\cdot}03$. (*a*) The bulk phase diagram as function of $D$ and $t$. Full lines: first order I/N, N/$S_A$ and I/N coexistence lines; dashed line: second order N/$S_A$ coexistence line. The circle denotes the tricritical point ($D_{crit}$, $t_{tri}$). (*b*) Nematic and smectic order parameter dependence on $t$ for different values of $D$. Full line: $D = 0$; dashed line: $D = 1{\cdot}1$; dash–dotted line: $D = 1{\cdot}5$. For $D = 1{\cdot}1$ and $D = 1{\cdot}5$, $s(t)$ curves coincide for $t - t_n > 0{\cdot}07$.

discontinuous at $t = t_n + \frac{2}{9}$. The tricritical point occurs at $D = D_{crit}$, and (scaled) temperature $t_{tri}$. These quantities are determined self-consistently by the relations

$$D_{crit} = \sqrt{(2C_2H)}, \tag{5a}$$

$$H = -t_{tri} + t_n + s_b/2, \tag{5b}$$

$$(rt_{tri} - t_S)^2 = 2s_b^2H/C_2, \tag{5c}$$

and

$$s_b = (\sqrt{[r - 4(t_{tri} - t_n)]})/2. \tag{5d}$$

Analytic evaluation of the position of the triple point is not possible, but it does show up in explicit numerical calculations. In figure 1 (*a*), we show a phase diagram as a function of $D$ and $t$, calculated for typical values of the liquid crystal constants. In figure 1 (*b*), the order parameter variation as a function of temperature is shown for different values of $D$. At $D = 1{\cdot}1$, both transitions are first order; by $D = 1{\cdot}5$ the N phase is no longer stable.

We note that an experimental realization of changing $D$ involves changing the aliphatic chain length in liquid crystalline molecules [4]. Thoen *et al.* [18], obtained an experimental phase diagram analogous to figure 1 (*a*), in which the coupling $D$ is increased by increasing $n$ in the homologous series of $n$CB compounds.

### 2.3. *Screw dislocation: parametrization and free energy*

In an inhomogeneous phase, $g(x)$ includes the $g_N^{non}$ and $g_S^{non}$ terms. These terms are necessarily non-zero in the presence of the screw dislocation. It is convenient to introduce dimensionless cylindrical coordinates $(\rho, \varphi, z)$, which define $\mathbf{x}$. The smectic phase is expressible as

$$\phi(\mathbf{x}) = z + u(\mathbf{x}) + M\varphi, \tag{6}$$

where the winding number M is an integer measuring the strength of the dislocation, and $u(\mathbf{x})$ is the layer displacement field. The presence of the dislocation is now indicated by the condition that far from the dislocation the smectic layers are undistorted, i.e. $u(\rho \to \infty) \to 0$. In this limit, other quantities take the values they would take in an undistorted smectic; we shall characterize these with a subscript b (bulk) (for example, $\varepsilon_b, s_b$). A more detailed discussion of the large scale structure of screw dislocations can be found in textbooks about defects in condensed matter physics [1, 2].

The director field $\mathbf{n}(\mathbf{x})$ can now be described by local spherical polar angles $\vartheta$, $\alpha$

$$\mathbf{n}(\mathbf{x}) = \mathbf{e}_\rho \cos\alpha \sin\vartheta + \mathbf{e}\varphi \sin\alpha \sin\vartheta + \mathbf{e}_z \cos\vartheta, \tag{7}$$

shown in figure 2.

This parametrization is then used to define the free energy. We confine our interest to dislocations in which the cylindrical symmetry is preserved; this seems a

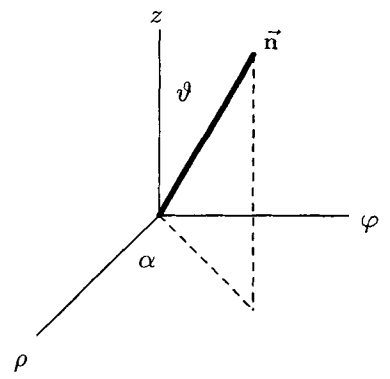


Figure 2. Definition of angles $\alpha$ and $\vartheta$ describing a local director field orientation.

reasonable assumption and certainly saves much additional mathematical complexity. We now obtain

$$g_N^{non} = s^2 H_N^{(1)} + \left(\frac{\partial s}{\partial \rho}\right)^2 H_N^{(2)}, \quad (8a)$$

$$g_S^{non} = \epsilon^2 H_S^{(1)} + \left(\frac{\partial \epsilon}{\partial \rho}\right)^2 H_S^{(2)}, \quad (8b)$$

where

$$\begin{aligned} H_N^{(1)}(\rho) = \frac{1}{2}\Bigg(&\frac{\sin^2\vartheta}{\rho^2}(\cos^2\alpha + a_2\sin^2\alpha\cos^2\vartheta \\ &+ a_3\sin^2\alpha\sin^2\vartheta) + \left(\frac{\partial\vartheta}{\partial\rho}\right)\frac{\sin(2\vartheta)}{\rho} \\ &\times(\cos^2\alpha + a_2\sin^2\alpha) + \left(\frac{\partial\vartheta}{\partial\rho}\right)^2 \\ &\times(\cos^2\alpha\cos^2\vartheta + a_2\sin^2\alpha \\ &+ a_3\cos^2\alpha\sin^2\vartheta) + \left(\frac{\partial\vartheta}{\partial\rho}\right)\left(\frac{\partial\alpha}{\partial\rho}\right) \\ &\times\frac{\sin(2\vartheta)\sin(2\alpha)}{2}(a_2 - 1) \\ &+ \left(\frac{\partial\alpha}{\partial\rho}\right)\frac{\sin(2\alpha)\sin^2\vartheta}{\rho}(-1 + a_2\cos^2\vartheta \\ &+ a_3\sin^2\vartheta) + \left(\frac{\partial\alpha}{\partial\rho}\right)^2\sin^2\vartheta(\sin^2\alpha \\ &+ a_2\cos^2\alpha\cos^2\vartheta + a_3\sin^2\vartheta\cos^2\alpha)\Bigg), \end{aligned} \quad (8c)$$

$$\begin{aligned} H_N^{(2)}(\rho) = \tfrac{1}{6}(&a_\parallel\sin^2\vartheta\cos^2\alpha + a_\perp(\cos^2\vartheta \\ &+ \sin^2\vartheta\sin^2\alpha)), \end{aligned} \quad (8d)$$

$$\begin{aligned} H_S^{(1)}(\rho) = \Bigg(&\frac{\partial u}{\partial\rho}\Bigg)^2(\sin^2\vartheta\cos^2\alpha + R(\sin^2\vartheta\sin^2\alpha \\ &+ \cos^2\vartheta) + \frac{M^2}{\rho^2}(\sin^2\vartheta\sin^2\alpha \\ &+ R(\sin^2\vartheta\cos^2\alpha + \cos^2\vartheta)) + 1 \\ &+ \cos^2\vartheta + R\sin^2\vartheta - 2\left(\frac{\partial u}{\partial\rho}\sin\vartheta\cos\alpha \right. \\ &\left. + \frac{M}{\rho}\sin\vartheta\sin\alpha + \cos\vartheta\right) \\ &+ (1 - R)\left(\frac{\partial u}{\partial\rho}\left(\sin(2\vartheta)\cos\alpha \right.\right. \\ &\left.\left. + \frac{M}{\rho}\sin^2\vartheta\sin(2\alpha)\right) + \frac{M}{\rho}\sin(2\vartheta)\sin\alpha\right), \end{aligned} \quad (8e)$$

$$H_S^{(2)}(\rho) = \sin^2\vartheta\cos^2\alpha + R(\sin^2\vartheta\sin^2\alpha + \cos^2\vartheta), \quad (8f)$$

and where $R = \gamma_\perp/\gamma_\parallel$ and $a_i = k_i/k_1\{i = 2, 3, \parallel, \perp\}$.

There are several important characteristic lengths involved in this problem. The most important of these are: the smectic coherence length $\xi_\perp = \sqrt{[RC_3/(2C_2)]}/\varepsilon_b$ the nematic twist ($i = 2$) and bend ($i = 3$) coherence lengths $\xi_i = \sqrt{(C_1 a_i)}$ and the nematic twist and bend penetration depths $\lambda_i = \xi_i/(\sqrt{[RC_3]}\varepsilon_b)$. The coherence lengths define a length scale over which a relevant perturbed order disappears. The penetration depths define the length scale on which twist and bend can penetrate into the $S_A$ phase.

The minimization of $g(\rho)$ gives rise to five coupled differential equations in the variables $s(\rho)$, $\varepsilon(\rho)$, $\alpha(\rho)$, $\vartheta(\rho)$ and $u(r)$. Details of these equations (and some further minor technical details concerning their solution) are relegated to Appendix A. We have solved these equations using standard relaxation techniques [23], and the resulting solutions are discussed in the next section.

## 3. Screw dislocation core structure

### 3.1. *Asymptotic behaviour*

We first study the asymptotic behaviour of the core structure. This should depend only on the elastic energy in the harmonic approximation; i.e. it only depends on smectic elastic constants. Far from the core, on length scales $\rho \gg \xi_\perp$, $\mathbf{n} \times \mathbf{a} = 0$, where $\mathbf{a}$ is a unit vector perpendicular to the smectic layers [24]; the molecules are perpendicular to the smectic layers. In this limit the smectic phase factor is $\phi_b(\rho) = \phi_b(\rho \to \infty) = z + M\rho$, yielding $\vartheta_b = \tan^{-1}(M/\rho)$ and $\alpha_b(\rho) = \alpha_b(\rho \to \infty) = \pi/2$. This result follows also from the continuum-like approach of Loginov and Terentjev [12]. The bulk values of the nematic order parameter $s_b$ and the smectic order parameter $\varepsilon_b$ are simply determined by minimizing the relevant bulk free energy contributions, $g_{bulk}$, defined in equation (4), with respect to $s$ and $\varepsilon$.

At the dislocation core axis, the topological requirements are incompatible with bulk smectic layering. Much further discussion of the structure must necessarily concern the way in which the frustration imposed by the winding number $M$ is resolved. However departures of the smectic and nematic order parameters from their bulk values are not so dependent. We find that $\delta s = s_b - s(\rho) \propto \rho^{-6}$ and $\delta\varepsilon = \varepsilon_b - \varepsilon(\rho) \propto \rho^{-4}$.

### 3.2. *Classification of different core structures*

The existence of a non-zero winding number $M$ compels the inner structure of the dislocation core to involve some departures of the order parameters from their bulk values, and indeed some regions where the order parameters disappear. The frustration seems capable of being resolved in one of three qualitatively different ways. We have labelled them, descriptively, as the 'double twist' (DT), the 'classical' (CL), and the 'broken polar symmetry' (BP) solutions. In the DT and CL solutions $\alpha(\rho) = \pi/2$ and $u(\rho) = 0$. Equivalently, the director at a point does not tip out of a plane perpendicular to the radius from the

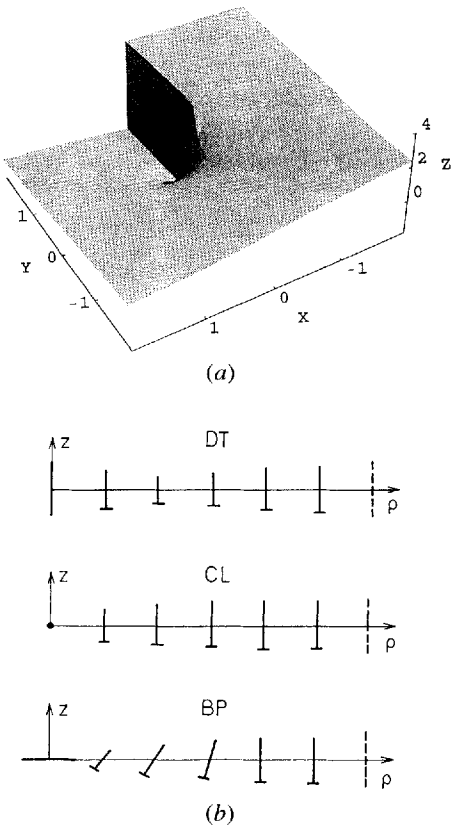


Figure 3. (*a*) A smectic layer surrounding a screw dislocation of strength $M = 1$ for the case $u(\mathbf{x}) = 0$. $x = \rho \cos \varphi$, $y = \rho \sin \varphi$, $\phi(\mathbf{x}) = M\varphi = M \tan^{-1}(y/x)$. (*b*) Schematic presentation of $\mathbf{n}$ in the DT, CL and BP solution in the $(\rho, z)$ plane. The nail presentation is used. The length of a nail is proportional to the length of the $\mathbf{n}$ projection in the $(\rho, z)$ plane. Nails with 'head' correspond to $\mathbf{n}$ with a finite component in the $\mathbf{e}_\varphi$ direction. The dot indicates the case $\mathbf{n} \| \mathbf{e}_\varphi$. Dashed nails present asymptotic orientation of $\mathbf{n}$ in the limit $\rho - > \infty$, where $\mathbf{n} \| \mathbf{e}_z$.

dislocation core to that point, and the layers do not distort from their asymptotic form (though, of course, they do reduce in intensity). In the BP solution all five variables appearing in the variational equations depend on position. A schematic picture of the screw dislocation core structure is shown in figure 3. In figure 3 (*a*) the layer structure is presented in the case when $u(\rho) = 0$ (DT or CL). The solutions differ most strongly in the nematic director $\mathbf{n}$ pattern within the core as depicted in figure 3 (*b*).

One interesting feature of the results in the core region appears to be independent of the details of the core structure. The defect topology forces the smectic order parameter $\varepsilon$ to be zero along the defect line itself (i.e. at $\rho = 0$). We find that $\varepsilon(\rho) \propto \rho^M$; thus $\varepsilon(\rho)$ in this region seems to depend on the homotopic classification of the defect, but to be independent of the detailed way in which the consequent frustration is resolved.

In the ensuing sub-sections we describe in detail results for the core structures of the three types of defect. We first concentrate on the case $D = 0$. The free energy of equation (1) admits an enormous parameter space, and in order to make reasonable progress it is necessary to restrict the set of values over which studies are made. We have chosen the following values of the model scaled parameters in equations (4) and (8), which are broadly speaking appropriate to an experimental $S_A$ phase

$$a_2 = a_3 = a_\parallel = a_\perp = 10;\ C_1 = 100;\ C_2 = 1;\ C_3 = 100;$$

$$R = 1;\ t_n = t_S = 50;\ r = 1{\cdot}03.$$

These calculations are carried out at scaled temperature $t = t_n - 1$. In Appendix B we discuss the criteria by which these parameters have been chosen.

### 3.3. *The DT core structure*

In this solution the core is singular only in the smectic (and not in the nematic) order parameter. Such a solution is sometimes known as a semi-defect [25]. The system avoids a smectic layer discontinuity along the core axis by a local transition into the nematic phase. The director $\mathbf{n}(\rho)$ remains continuous and well-defined. For $\rho \ll \xi_\perp$, the nematic director tends to point along the dislocation axis, and it is easy to show that in this region $\vartheta(\rho) \propto \rho$.

As $\rho$ is decreased from $\infty$, $\mathbf{n}$ first twists one way ($\vartheta$ increase if $M > 0$), before turning and twisting the other way, so that, at $\rho = 0$, $\mathbf{n}$ is parallel to its direction at $\rho = \infty$. It is for this reason that this structure is known as a 'double twist' solution. In figure 4 (*a*), we plot the dependence of $\vartheta(\rho)$, for $M = 1, 2$, showing the maximum in $\vartheta(\rho)$, and compare this solution to the elastic harmonic solution which follows from prescribing $\mathbf{n} \| \mathbf{a}$.

In the $D = 0$ case, the weak coupling between smectic and nematic order has the effect that the nematic order parameter s is only weakly dependent on $\rho$. This dependence is shown in figure 4 (*b*). Nevertheless, solutions with this basic structure exist for any reasonable choice of the liquid crystal material constant values.

Further interesting information can be obtained from examining the free energy density profile. This quantity should be examined with caution, because $g(\rho)$ is a non-local quantity; some parts of it can be transformed into surface contributions using the divergence theorem. Nevertheless, some insight into the relative distribution of the elastic forces can be obtained. In figure 5 we plot $\Delta g(\rho) = g - g_b$, for $M = 1, 2$. The major contribution comes from $g_S^{non}$; this is despite the rather small actual change in the smectic order parameter. For $M > 1$, there is also a noticeable contribution from $g_N^{non}$ in the region $\rho < \xi_\perp$. This is because the $\varepsilon \propto \rho^M$ dependence increasingly expels smectic order from a central core, and hence suppresses the relative importance of changes in this order

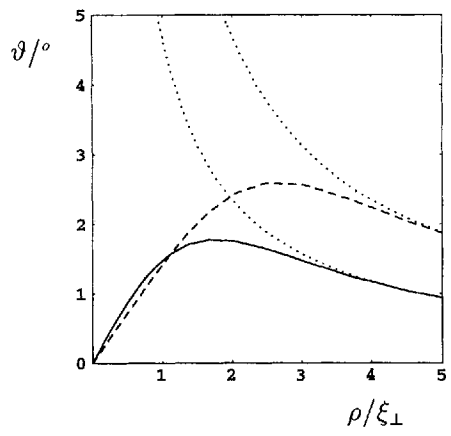


(*a*)

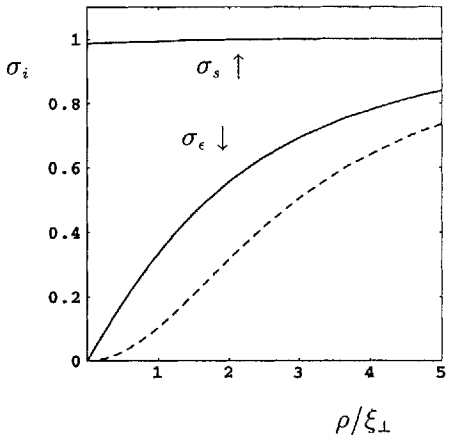


(*b*)

Figure 4. Core structure of the DT solution. Full Line: $M = 1$; dashed line: $M = 2$. $C_1 = 100$, $a_i = 10$ ($i = 2, 3, \perp, \parallel$); $C_2 = 1$, $C_3 = 100$, $R = 1$; $t_n = t_s = 50$, $r = 1{\cdot}03$, $t - t_n = -1$. (*a*) Dependence of $\vartheta(\rho)$ compared to the continuum solution $\vartheta_b(\rho)$ (described by the dotted line). (*b*) A scaled order parameter $\sigma_i$, $i = (\varepsilon, s)$, as function of $\rho$. $\sigma_\varepsilon = \varepsilon/\varepsilon_b$, $\sigma = s/s_b$. Differences between $\sigma_s(\rho)$ for $M = 1$ and $M = 2$ are negligible.

parameter. This effect is demonstrated in the inset to figure 5; the main elastic effect close to the core now comes from the twist deformation.

### 3.4. *The CL core structures*

The core structure of the CL (classical) solution is a 'full defect' [25]; both nematic and smectic order parameters are singular along the core axis. In all cases, close to the core axis, **n** lies in the $\mathbf{e}_\varphi$ direction. This fact forces a singularity in the nematic order parameter. Thus the dislocation core essentially consists of isotropic fluid, surrounded by an annuloid of nematic, in turn surrounded by bulk smectic phase. The nematic defect is a wedge (and not a twist) defect of order 1.

We call this structure classical because the classical prediction for $\vartheta = \tan^{-1}(M/\rho)$. In this context the classical solution is the solution in the asymptotic region of large $\rho$ as calculated by continuum theory. This leads to $\vartheta = \pi/2$ at $\rho = 0$; in this case $\mathbf{n}(\rho \to 0)$ points in the $\mathbf{e}_\varphi$ direction.

In the CL solution, the nematic director **n** tends to be perpendicular to the smectic layers; its behaviour is reminiscent of the elastic continuum solution. The nematic core is smaller than in the DT case, apparently because this structure is more consistent with the smectic layers. The smectic order can therefore persist closer to the core region. It is possible to derive qualitative results for the radii $\rho_C^I$ of the isotropic and $\rho_C^N$ of the nematic core regions. For the choice of parameters discussed in § 3.2 above, we find $\rho_C^I/\xi_\perp \approx 0{\cdot}3M^{2/3}$ and $\rho_C^N \approx 0{\cdot}3M$. This is broadly in agreement with the more accurate numerical results, so long as $a_\perp, a_\parallel < 10$. An interesting feature of our results is that $\rho_C^N \propto 1/\sqrt{\varepsilon_b}$. This has the effect that close to the N–$S_A$ transition for $D < D_{crit}$ (i.e. when the transition is continuous), $\rho_C^N$ diverges.

In order to obtain stable CL solutions for $M = 1$ and $M = 2$, we have found it necessary to consider rather large values of $a_3 = K_3/K_1 \approx 30$. In fact, the existence of a CL solution demands a favourable combination of a number of circumstances. We postpone this discussion until § 4.

Figures 6 and 7 reveal structural details of the CL core structure for $M = 1$ and $M = 2$. In figure 6 (*a*) we plot $\vartheta = \vartheta(\rho)$. The angle $\vartheta$ monotonically decreases from $\vartheta(0) = \pi/2$ towards $\vartheta(\infty) = 0$ in a fashion very similar to that predicted by the continuum solution. In the inset to figure 6 (*a*) we show departures of $\vartheta(\rho)$ from the continuum solution $\vartheta_b(\rho) = \tan^{-1}(M/\rho)$. In the core region the deviations extend up to ~8 per cent for the chosen set of parameter values. The corresponding smectic and nematic order parameter behaviour is plotted

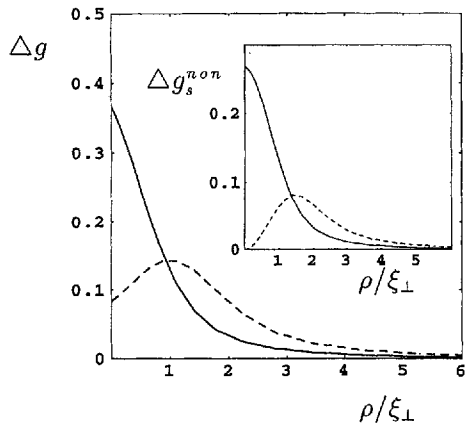


Figure 5. The free energy density plot $\Delta g(\rho) = g(\rho) - g_b$ for the DT solution. Full line: $M = 1$; dashed line: $M = 2$. In the inset we show the corresponding $\Delta g_s^{non}(\rho) = g_s^{non}(\rho) - g_b$. Values of parameters are as in figure 4.

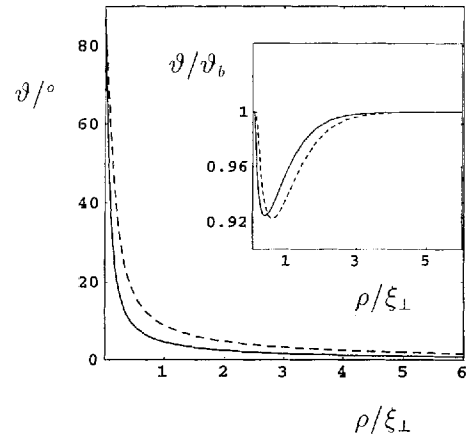


(*a*)

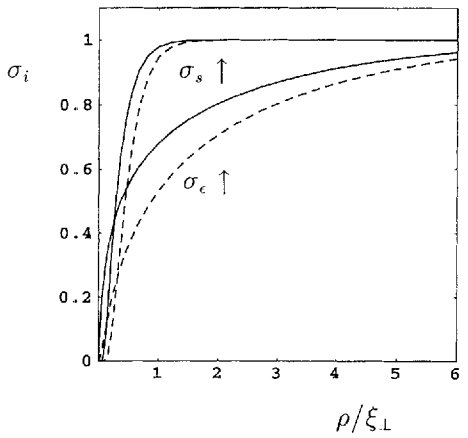


(*b*)

Figure 6. Core structure of the CL solution. Full line: $M = 1$; dashed line: $M = 2$. Values of parameters are as in figure 4, except $a_3 = 30$. (*a*) $\vartheta(\rho)$ dependence. Inset: the ratio $\vartheta(\rho/\vartheta_b(\rho)$ describing departures from the continuum approach. (*b*) A scaled order parameter $\sigma_i$, $i = (\varepsilon, s)$, as a function of $\rho$. $\sigma_\epsilon = \varepsilon/\varepsilon_b$, $\sigma = {}_S = s/s_b$.

in figure 6 (*b*). At the dislocation axis, necessarily $s(0) = 0$ and $\varepsilon(0) = 0$. Some further information can be seen in figure 7, where the free energy density profile $\Delta g(\rho) = g(\rho) - g_b$ is shown. By contrast with the DT solution, the major contribution comes from the nematic part of the free energy. The Frank elastic energy is dominated by the bend contribution. As in the DT solution the $g_S^{non}(\rho)$ dependence is qualitatively different for $M = 1$ and $M > 1$ due to the $\varepsilon \propto \rho^M$ dependence of the smectic order parameter close to the dislocation axis. This is demonstrated in the inset to figure 7.

### 3.5. *The BP core structure*

In the BP solution both nematic and smectic components are singular along the core axis. The nematic director field emerges radially from the dislocation axis and

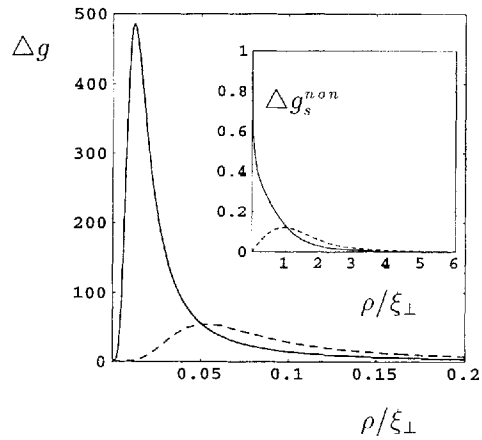


Figure 7. The free energy density plot $\Delta g(\rho) = g(\rho) - g_b$ of the CL solution. Full line: $M = 1$; dashed line: $M = 2$. Inset: $\Delta g_S^{non}(\rho) = g_S^{non}(\rho) - g_b$. Values of parameters are as in figure 4.

approaches its bulk value in a splay-like way. This causes the smectic layers to adopt qualitatively different structures compared to the DT and CL solution; the layers orient perpendicular to the axis close to the defect origin. The layers can approach this orientation in one of two ways; the layers can tip either up or down. In this sense the polar or up-down symmetry of the defect is broken. For each solution $u(\rho)$, there is an equivalent $\tilde{u}(\rho) = -u(\rho)$. Because of this property we call this solution broken polar symmetry.

In the BP solution all variational parameters of our model exhibit spatial variation. This is shown in figure 8 for $M = 1$. The nematic director field evolves from the radial configuration $\mathbf{n}(0) = \mathbf{e}_\rho$ at $\rho = 0$ into $\mathbf{n}(\infty) \| \mathbf{a} \sim \mathbf{e}_z$ far from the dislocation axis. The corresponding angle $\vartheta(\rho)$

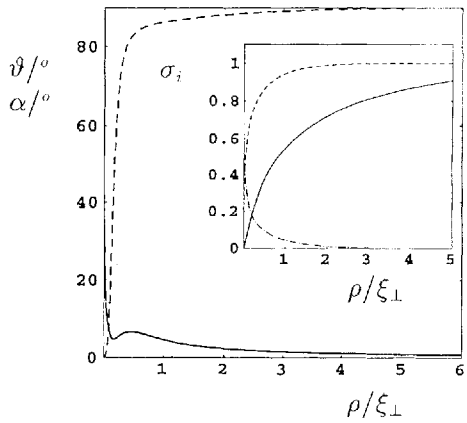


Figure 8. Core structure of the BP solution. Full line: $\vartheta = \vartheta(\rho)$; dashed line: $\alpha = \alpha(\rho)$. Inset: $\sigma_i$ spatial dependence, $i = (s, \varepsilon, u)$. Full line: $\sigma_\epsilon/\varepsilon_b$, dashed line; $\sigma_s = s/s_b$, dash–dotted line; $\sigma_u = u$. Values of parameters are as in figure 4, except $a_2 = 1$, $a_3 = 30$.

decreases from $\vartheta(0) = \pi/2$ towards $\vartheta(\infty) = 0$, and $\alpha(0) = 0$ towards $\alpha(\infty) = \pi/2$. The 'escape' of smectic layers at $\rho = 0$ is demonstrated via $u(\rho)$ in the inset to figure 8 together with the $s(\rho)$ and $\epsilon(\rho)$ spatial dependence. Because of the full defect character of the CL core structure, both order parameters drop to zero at $\rho = 0$.

The BP solution can be obtained only for large anisotropy of $a_2$ and $a_3$ ratios, i.e. $a_2 \ll a_3$. In our calculation we set $a_2 = 1$, $a_3 = 30$. With increased $a_2$ or decreased $a_3$ value, the region corresponding to a radial **n** distribution rapidly shrinks, ruling out the escape of smectic layers. In the case shown in figure 8, the BP structure and DT structure resemble each other in the range $\rho/\zeta_\perp > 0{\cdot}2$. If $a_3$ is increased further, the BP solution becomes more reminiscent of the CL solution. In the next section we discuss that circumstances under which this structure could be stabilized.

## 4. Stability and existence of core structures

### 4.1. *General consideration*

In this sub-section we discuss the existence and stability of different core structures.



#### 4.1.1. *Existence*

The DT structure seems to exist for any reasonable set of parameters. It is more difficult to find the CL solution. Our intuitive expectation was that its existence is permitted if the nematic bend coherence length $\xi_3$, the smectic coherence length $\xi_\perp$ and the bend penetration length $\lambda_3$ are comparable. This situation allows the relatively cheap large bend deformation field which exists in this case in the core region. In the core region, the tendency of **n** to be parallel to the layer normal **a** is weakened. However, our calculations seem to show that the situation is more complex than this. Indeed we do not at this stage understand all the relevant mechanisms.

To obtain the CL solution, we had to choose relatively large values of $R = \gamma_\perp/\gamma_\parallel = 1$ and $a_3 = K_3/K_1 = 30$. A large value of $\gamma_\perp$ tends to orient **n** along **a** and that is indeed consistent with the CL director pattern. The condition $\mathbf{a}_3 \gg 1$ increases the bend penetration length $\lambda_3$. If these conditions are not met in our solutions we obtain a structure which we call the undeveloped CL solution. In this solution, the director field is reminiscent of the DT solution, but abruptly reorients along $\mathbf{e}_\varphi$ at the dislocation axis. However, this solution is stabilized by the CL solution boundary condition constraint $\mathbf{n}(0) = \mathbf{e}_\varphi$. Because there is no physical mechanism responsible for the abrupt director reorientation close to $\rho = 0$ in the undeveloped CL solution, we believe that this solution does not correspond to a free energy local minimum. We find that under specific circumstances, the CL solution continuously evolves into the undeveloped CL solution. This was achieved by decreasing $a_3$. We believe that by removing the constraint $\mathbf{n}(0) = \mathbf{e}_\varphi$, this phenomenon would result in a continuous CL–DT structure transformation. In the intervening structure, $\vartheta(0)$ would continuously transform from $\vartheta(0) = \pi/2$ (CL solution) to $\vartheta(0) = 0$ (DT solution), where the defect in the nematic component vanishes.

To obtain the BP solution we have to introduce an anisotropy in the $K_2$ and $K_3$ Frank elastic constants. In our case, we have taken a rather extreme limit, in which $a_2 = 1$, $a_3 = 30$. If the anisotropy among the constants is then decreased, the $\alpha(\rho) \neq$ constant solution characteristic of the BP structure, no longer exists. Analogous conclusions were reached by Press and Arrott [26], and by Williams [27] in their respective studies of nematic profiles in cylindrically and spherically shaped cavities. They observed symmetry breaking in the nematic field reminiscent of that in **n** of the BP structure, when anisotropy between Frank nematic elastic constants was introduced.

#### 4.1.2. *Stability*

We first discuss the stability of the DT and CL solutions. Transitions between these structures can be induced in a number of different ways. In most cases we expect the transition to be discontinuous. However, as we have already discussed above, a continuous transition is not ruled out on symmetry grounds.

The main difference between the two structures is that the CL structure is also singular in the nematic director field. This suggests that the energy balance between the structures depends on location in the $(D, t)$ phase diagram, shown in figure 1 $(a)$. If there is a nematic gap intervening between the $S_A$ and I phases the paranematic (essentially isotropic) phase close to the defect axis of the CL solution is energetically costly. In this case, the DT solution with nematic core is preferred. The situation changes, however, in the region of $S_A$ stability, where the nematic phase is less favoured than the isotropic phase. In our model, this regime corresponds to a temperature within the interval $[T_{NI}, T_{SI}]$ and the coupling constant $D$ is larger than its triple-point value $D_{tp} \sim 1{\cdot}28$. In this regime, the paranematic core of the CL solution becomes advantageous. But before reaching a definite conclusion, it is necessary to make a quantitative study of the effect of the coupling constant on the core structures.

The other important properties relevant to core structure are the different nematic and smectic elastic properties of the material. We first discuss the nematic Frank-elastic contributions. In the CL solution the bend deformation is dominant, whereas twist deformation dominates in the DT solution. A large value of the ratio $K_2/K_3$ therefore favours the CL director field. We note however the apparent paradox that a decreased $K_3$ increases the stability of the CL solution, but, as discussed in the previous sub-section makes it less likely to exist. The smectic elastic constants

are also relevant. A large value of $\gamma_\perp/\gamma_\parallel$ favours the CL solution, which has **n** closer to the smectic layer normal **a**. We have seen in § 3 that the core of the CL structure in smaller than that of the DT structure because the director field of the CL structure is more compatible with the smectic layer configuration. However, the DT structure has lower nematic elastic distortions. The nematic and smectic elastic distortions are weighted by constants $C_1$ and $C_3$, defined in equation (3), respectively. Therefore a large $C_3/C_1$ ratio favours the CL solution. To summarize, we expect the CL is favoured with respect to the DT structure for relatively large ratios of $C_3/C_1$, $K_2/K_3$ and $\gamma_\perp/\gamma_\parallel$ and in addition for $T > T_{NI}$ when $T < T_{SI}$.

We now discuss the stability of the BP structure. First we treat the regime where the DT structure is energetically more favourable than the CL solution. In this case, we do not expect the BP structure to be stable for the following reasons: (i) it has an isotropic core; (ii) its existence requires $K_2 \ll K_3$ and a low $K_2$ value favours the DT solution, and in the BP solution all the Frank nematic elastic distortions are present and are of comparable magnitude; (iii) the BP structure has an additional strong nematic elastic contribution due to the large gradient of the nematic order parameter; (iv) the outer core region of the DT and BP structure is similar and therefore cannot play decisive role.

The only possibility, therefore, for the existence of the BP structure, is the regime where the CL structure is favoured. In both the CL and BP structures, the core region is essentially isotropic. An important determinant of the stability is the structure of the smectic–isotropic interface at the edge of this core region. This interface can be thought of as a complex structure consisting of a N–I interface and an S–N interface. In the S–N interface, $\nabla\psi$ is always perpendicular to the interface. However, in the N–I interface, the BP structure has **n** more radial than the CL structure. Thus in the CL structure **n** is tangential to the interface, whereas in the BP case, **n** has perpendicular component. Now the structure of this interface is governed, as can be seen in equations (1), by the elastic constants $k_\parallel$ and $k_\perp$. If $k_\perp > k_\parallel$, the director should be perpendicular to the interface, favouring the BP solution.

### 4.2. *Numerical results*

In this sub-section, we examine quantitatively some of the hypotheses we have put forward in the previous sub-section. The most questionable hypothesis concerns the importance of position in the $(D, t)$ phase diagram on the core structure. For this reason we study the influence of the coupling constant $D$ on the CL and DT structures which exist for the conventional parameter values.

In order to show a global effect of $D$ on the core structure we define

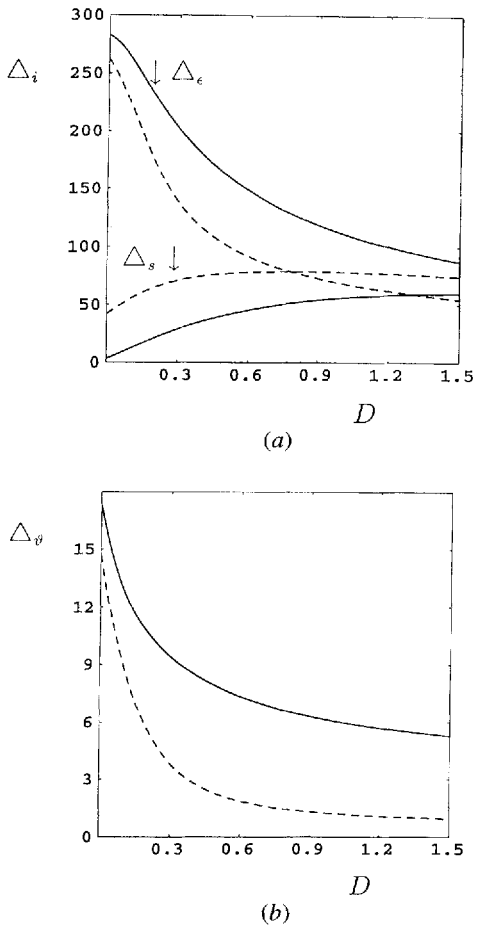


Figure 9. The effect of $D$ on the core structure. Full line: DT structure; dashed line: CL structure. Material constants are given in figure 4 with the exception that $a_2 = a_3 = 30$. (*a*) $\Delta_S$(cs) and $\Delta_\epsilon$(cs) as function of $D$. (*b*) $\Delta_\vartheta$(cs) variation with $D$.

$$\Delta_s(\mathrm{cs}) = \int_0^\infty (s(\rho) - s_b)d\rho,$$

$$\Delta_\epsilon(\mathrm{cs}) = \int_0^\infty (\epsilon(\rho) - \epsilon_b)d\rho,$$

$$\Delta_\vartheta(\mathrm{cs}) = \int_0^\infty (\vartheta(\rho) - \vartheta_b)d\rho. \qquad (9)$$

Here cs in brackets describes the specific core structure (cs = (DT, CL)). The quantities $\Delta_S$(cs) and $\Delta_\epsilon$(cs) describe departures of the nematic and smectic order parameter from its bulk value, respectively. The departure of the director field from the classical solution is measured by $\Delta_\vartheta$(cs).

The influence of $D$ on the core structure of the DT and CL solution is demonstrated in figure 9. We see that at higher values of $D$, $\Delta_S$(cs) and $\Delta_\epsilon$(cs) values are closer. This indicates that for a given structure, the profiles $s(\rho)$ and $\varepsilon(\rho)$ become similar. The departures of $s(\rho)$ from the

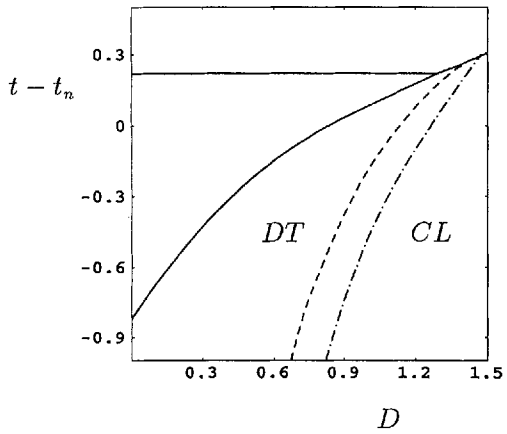


Figure 10. The stability diagram of the DT and CL solution in the $(t, D)$ plane. Dashed line: $R = 1$; dash–dotted line: $R = 0{\cdot}8$. The values of remaining constants are as in figure 4 except that $a_3 = 30$.

bulk value are increased, whereas those of $\varepsilon(\rho)$ decreased. The overall effect is that the core size is reduced. In addition, the spatial dependence of the order parameter in both structures becomes similar. The dependence of $\Delta_\vartheta$(cs) also decreases with increased $D$, indicating that in both structures, on average, the director profile is closer to the layer normal. This is due to the reduced core size in which departures of **n** from **a** are significant. Note that for large values of $D$, the paranematic (weakly developed nematic) phase exists in both structures. Therefore temperature, i.e. position in the $(D, t)$ phase diagram, is not as important in the stability considerations as we had expected.

The stability regions of the CL and DT solution in the $(t, D)$ plane are shown in figure 10. At low temperature and low values of $D$, the DT structure is stable in agreement with our previous discussion. With increased $D$ at constant temperature, the elastic components of the two structures become increasingly similar. As a result, the free energy is determined by the size of the region in which the smectic order parameter is reduced. Since the CL solution has a narrower core, at a critical value of $D = D_c(t)$ the DT solution discontinuously transforms into the CL solution. Then the graph $D_c(t)$ describes the coexistence line of the two dislocation structures in the $(D, t)$ plane.

However, if the temperature is then increased, the DT structure is re-entered if the value of $D$ is below some critical value $D_{max}$. The calculations show that in both structures the elastic contributions are comparatively less decreased than the expelled phase contribution with increased t. As a consequence the stability region of the DT structure is increased, because the competition among elastic terms favours the DT structure. For $D > D_{max}$ the CL solution is stable in the whole temperature range of the $S_A$ phase existence.

In figure 10 we show the stability diagram for different ratios of $R = \gamma_\parallel/\gamma_\perp$. As expected the stability regime of the CL structure is increased for increased $R$. Increasing the ratio $K_2/K_3$ has a similar effect. However, we find that the BP structure is not stable in any regime for the chosen set of parameters, and we speculate that in fact this structure is never stable.

### 4.3. *Dislocations with higher M*

We now discuss the free energy dependence of the core structure on the winding number $M$. In particular, we stress some differences between the defects we discuss in this paper and analogous phenomena in nematic liquid crystals, for which there is already a well-developed body of theory.

In a conventional continuum theory, calculating a free energy cost $\Delta F$ of a dislocation involves introduction of a core radius $\rho_c$ (also called a cut-off radius). This separates the core region, where the continuum approach fails, from the surrounding region. The corresponding free energy is then $\Delta F = F_{core} + F_e$. The quantities $F_{core}$ describe contributions from the core and $F_e$ from the surrounding region. The elastic term $F_e$ can be calculated in the continuum limit.

It is worthwhile to recall the importance of these free energy terms in the case of dislocations in a nematic liquid crystal. Nematic dislocation lines are conventionally characterized by an index. $S$. Clearly there is a close analogy between the index $S$ and the winding number $M$ describing the screw dislocation. For a dislocation of a strength $S$, the nematic director orientation changes by $2\pi S$ on going around the dislocation. The apolar symmetry of the nematic orientational order allows $S = (0, \pm\frac{1}{2}, \pm 1, \ldots)$. In a nematic fluid, the $F_e$ contribution is dominant. In most cases [4] $F_e(S) = S^2 F_e(1)$. As a consequence a dislocation of a high index $S$ rarely exists. It is energetically more convenient for a high $S$ dislocation to dissociate into $N$ dislocations of lower index $S_i$, obeying the conservation rule $S = \Sigma_i^N S_i$.

In the case of the screw dislocation, the behaviour is essentially different. From the continuum theory, it follows [12, 13] that $F_e \approx 0$. Thus the free energy costs are given by $\Delta F \approx F_{core}$.

We now estimate $\Delta G$, the dimensionless free energy cost per unit length $\Delta G$ of the screw dislocations in the case $D = 0$. We write it as a sum of the expelled smectic phase contribution $G_{exp}$ and elastic distortion contribution $G_e$

$$\Delta G = G_{exp} + G_e, \tag{10}$$

$$G_{exp} = 2\pi \int_0^\infty (g_N^{loc} + C_2 g_S^{loc} - g_{bulk})\rho \, d\rho, \tag{10a}$$

$$G_e = 2\pi \int_0^\infty (C_1 g_N^{non} + C_3 g_S^{non})\rho \, d\rho. \tag{10b}$$

Other quantities in equations (10) are given in equations (3), (4) and (8).

To estimate the expelled phase contribution $G_{exp}$ we define the core radius $\rho_C^N$ of the $S_A$/N interface and $\rho_C^I$ of the N/I interface. The latter exist only for the full defect core structure. Assuming that the order parameters take their bulk values in relevant regions, we obtain

$$G_{exp} = (\rho_C^I)^2 \pi |g_N^{loc}| + (\rho_C^N)^2 \pi C_2 |g_S^{loc}|. \quad (11)$$

The values of the core radii depend on $M$. A simple asymptotic analysis shows that for the CL solution- $\rho_C^N(M) = M\rho_C^N(1)$, $\rho_C^I(M) = M^{2/3}\rho_C^I(1)$. Consequently,

$$G_{exp}(M) = M^{4/3}|g_N^{loc}|\pi(\rho_C^I(1))^2 + M^2 C_2 |g_S^{loc}|\pi(\rho_C^N(1))^2. \quad (11a)$$

Figure 4 (*b*) indicates that $\rho_C^N(M) = M\rho_C^N(1)$ also applies for the DT structure, for which

$$G_{exp}(M) = M^2 C_2 |g_S^{loc}|\pi(\rho_C^N(1))^2. \quad (11b)$$

The $G_{exp}(M)$ shows a stronger than linear dependence on $M$ in both structures. As a consequence $G_{exp}(2) > 2G_{exp}(1)$. We see that the expelled phase contribution favours the formation of several low $M$ dislocations.

Finally, we have to estimate the elastic contribution $G_e$, which the numerical calculations show plays the dominant role. We confine our interest to the DT structure, in which the nematic elastic distortions are negligibly small as compared to the smectic distortions. For simplicity we set $\gamma_\parallel = \gamma_\perp$, obtaining

$$G_e \approx 2\pi C_3 \int_0^\infty g_S^{non} \rho \, d\rho \approx 2\pi C_3 \int_0^{\rho_C^N} \left( \epsilon^2 (H_S^{(1)} + \left(\frac{\partial \epsilon}{\partial \rho}\right)^2 \right) \rho \, d\rho. \quad (12a)$$

We further approximate spatial dependence of the smectic order parameter by $\varepsilon(\rho < \rho_C^N) = \varepsilon_b \rho/\rho_C^N$, $\varepsilon(\rho \geq \rho_C^N) = \varepsilon_b$, and the $H_{(S)}^{(1)}(\rho)$ dependence roughly by $H_S^{(1)}(\rho < 1) = M^2/\rho^2$ and $H_S^{(1)}(\rho \geq 1) = M^2/(4\rho^4)$. The latter approximation assumes that $\vartheta(\rho < 1) \propto \rho$ and $\vartheta(\rho > 1) \approx \tan^{-1}(M/\rho)$. Now we obtain

$$G_e(M) \approx \frac{C_3 M^2 \pi \epsilon_b^2}{(\rho_C^N(M))^2} \left(1 + \frac{\ln(\rho_C^N(M))}{2}\right) = \frac{C_3 \pi \epsilon_b^2}{(\rho_C^N(1))^2} \left(1 + \frac{\ln(\rho_C^N(M))}{2}\right). \quad (12b)$$

We see that the elastic part $G_e$ depends only weakly on $M$. By contrast with $G_{exp}$, the elastic contribution prefers formation of one high $M$ dislocation rather than several dislocations with $M = 1$. What actually occurs thus depends on the relative importance of $G_e$ and $G_{exp}$.

This rough estimation is in accordance with our numerical results. In the regime studied, we get for the DT solution $2\Delta G(M = 1) \approx \Delta G(M = 2)$, and for the CL solution $2\Delta G(M = 1) > \Delta G(M = 2)$.

In this context it is also important to mention that in practice it turned out to be difficult to get the CL solution for $M > 1$. We suspect that this results from the different dependence of typical relevant lengths on $M$. The anisotropy between them is increased with $M$. As a consequence we fall into the regime where the CL solution cannot exist. To get the CL solution for $M = 2$, $a_3$ must be increased, and consequently also the bend penetration depth and nematic bend correlation length.

## 5. Inherent chirality

We have emphasized the importance of the screw dislocation core structure in the context of understanding the TGB phase. This phase may be stable if the liquid crystal has some inherent chirality. A typical phase diagram would have temperature along one axis and inherent chirality along the other. However in practice, the inherent chirality is modified by changing the ratio of left-handed to right-handed conformers in a mixture of conformers with competing chirality. In this case the coupling between the chirality and the nematic twist deformation field confined to the screw dislocation core structure can affect the core structure itself. Indeed, if the coupling is strong enough, it may be that this can lead to partial phase separation of the conformers. This can in turn affect the region in which the TGB phase is stable as a function of temperature and concentration.

In order to check this hypothesis we add a chiral term [7] $\Delta f_{chol}$ to equation (1)

$$\Delta f_{chol} = -K_2 q_{chol} \mathbf{n} \cdot \nabla \times \mathbf{n}. \quad (13)$$

This contribution forces liquid crystal molecules to twist with respect to each other forming a helix of periodicity $q_{chol}$. We further consider the simple case when the inherent chirality results from the competition of a mixture of otherwise identical left- and right-handed chiral molecules whose concentrations are described by $c_l(\rho)$ and $c_r(\rho)$, respectively. Thus

$$q_{chol} = q_{max} \Delta c(\rho), \quad (14)$$

where $\Delta c = c_l - c_r$ and $q_{max}$ corresponds to a maximal value of $q_{chol}$.

We must now add an additional contribution $\Delta f_{mixt}$ to equation (1) to take account of the free energy of mixing. This takes into account the chemical potentials $\mu_l$, $\mu_r$ of the left- and right-handed conformers, respectively, and an entropic term of mixing

$$\Delta f_{mixt} = -\mu c_l - \mu_r c_r + kT\rho_0 c_l \ln c_l + kT\rho_0 c_r \ln c_r, \quad (15)$$

where $\rho_0$ describes the particle-density and $k$ is the Boltzmann constant.

We shall consider a simple problem in which $\mu \equiv \mu_l = \mu_r$, and thus $\Delta c = 0$ in the homogeneous case. We are thus considering a screw dislocation in a non-chiral $S_A$ fluid which can become locally chiral under the influence of twist.

Taking into account $c_l + c_r = 1$, equation (15) simplifies to

$$\Delta f_{\text{mixt}} = -\mu + kT\rho_0 \left( \frac{1+\Delta c}{2} \ln \left( \frac{1+\Delta c}{2} \right) + \frac{1-\Delta c}{2} \ln \left( \frac{1-\Delta c}{2} \right) \right). \quad (15a)$$

We may discard the $\mu$ contribution which only shifts the energy scale and treat $\Delta c(\rho)$ as an additional variational parameter. We use the scaling introduced in § 2.1, and now express the total dimensionless free energy density $g_{\text{tot}}$ as

$$g_{\text{tot}} = g + \Delta g_{\text{chol}} + \Delta g_{\text{mixt}}, \quad (16)$$

where

$$\Delta g_{\text{chol}} = -C_1 s^2 \gamma_t a_2 \Delta c \mathbf{n} \cdot \nabla \times \mathbf{n}, \quad (16a)$$

$$\Delta g_{\text{mixt}} = C_4 t \left( \frac{1+\Delta c}{2} \ln \left( \frac{1+\Delta c}{2} \right) + \frac{1-\Delta c}{2} \ln \left( \frac{1-\Delta c}{2} \right) \right), \quad (16b)$$

and $g$ is defined by equation (2). In equations (16) we have introduced the following new dimensionless constants: the twisting power $\gamma_t = q_{\max}/q_0$ and $C_4 = \rho_0 k T_{\text{NI}} c^2/(b^2 a_0)$. Typical values of these constants are $\gamma_t \sim 10^{-3}$ and $C_4 \sim 1$.

The minimization of $g$ with respect to $\Delta c$ yields

$$\Delta c(\rho) = \frac{\exp[\kappa(\rho)] - 1}{\exp[\kappa(\rho)] + 1}, \quad (17)$$

where

$$\kappa(\rho) = \frac{2C_1 s^2 a_2 \gamma_t}{C_4 t} \mathbf{n} \cdot (\nabla \times \mathbf{n}). \quad (17a)$$

We see that a spatially dependent twist deformation field induces spatial variations in $\Delta c(\rho)$; for a left hand twist $\mathbf{n} \cdot \nabla \times \mathbf{n} > 0$ and $c_l > c_r$. The $\Delta c(\rho)$ variation in turn affects the director field. The corresponding changes to the Euler–Lagrange equations are presented in Appendix A. The corrections are of order $\gamma_t$. For a typical case, where $\gamma_t \sim 10^{-3}$, they play a negligible role.

In previous sections we have seen that under normal circumstances only the DT or CL solutions are stable. Since the twist elastic component dominates the DT structure, we confine our attention to this case.

In equations (17), the low $\kappa$ limit leads to a linear response regime in which

$$\Delta c(\rho) = \frac{C_1 a_2 s^2 \gamma_t}{2C_4 t} \mathbf{n} \cdot \nabla \times \mathbf{n}, \quad (18)$$

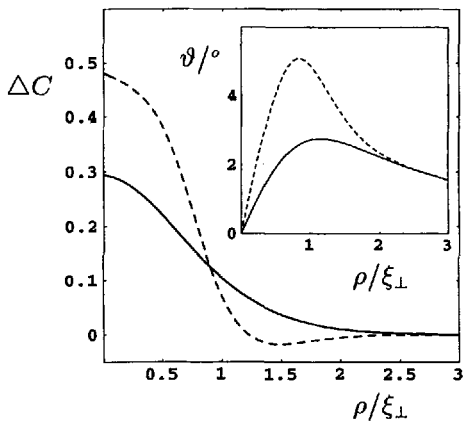


Figure 11. Spatial variation of $\Delta c(\rho)$ induced by the DT core structure. In the inset, the feedback effect is shown. Full line: $\gamma_t = 0{\cdot}001$; dotted line: $\gamma_t = 0{\cdot}05$. $(C_1 a_2 \gamma_t)/(2C_4 t) = 1$ and other parameters are as in figure 4.

where the twist is calculated in the absence of the mixing free energy terms. In practice this seems to be the regime of interest.

We see that twist director field locally enhances the conformer concentration with the same handedness. For very high values of $\gamma_t$, there can be a feedback effect, in which the handedness favours twist in the relevant direction.

The influence of the DT configuration on $\Delta c(\rho)$ has been plotted in figure 11. The twist changes direction at the core boundary and $\Delta c(\rho)$ follows this change. Since the reverse twist near the core edge is much more gradual than the twist at the core axis, this oscillation is not evident in the case shown with the full line. The influence of the variation in $\Delta c(\rho)$ and $\vartheta(\rho)$ is shown in the inset. In order to see this clearly, we have chosen an exaggerated value of $\gamma_t$. We see that inherent twist enhances the concentration with the same handedness which in turn increases the twist. For $\gamma_t = 0{\cdot}05$, the twist near the core axis is approximately twice that occurring in the case $\gamma_t = 0{\cdot}001$, where the feedback effect is negligible.

## 6. Conclusions

We have studied the core structure of a screw dislocation in the $S_A$ phase in the frame of the Landau–de Gennes theory. Understanding the screw dislocation core structure is of particular interest in the context of the recent discovery of the TGB phase, in which this dislocation plays the crucial role. Previous theoretical investigations of the screw dislocation are based either on the analogy [11] between the screw dislocation and vortex in the theory of superconductivity or the elastic [12] continuum approach. Neither of these studies allows strong nematic distortions close to the dislocation axis. In our study we

relax this constraint, which allows the possibility of spatial variation of the nematic orientational order parameter.

We have found three qualitatively different solutions which we name double twist (DT), classical (CL), and broken polar (BP) solution. The DT core structure is a semi-defect [24], i.e. it is singular only in the smectic phase $\phi(\mathbf{r})$. By contrast, the cores of the CL and DT structures form a full defect. At the dislocation axis they are, in addition, singular in the nematic director field. The CL and DT structures have a 'conventional' layer structure in which layers rotate in a staircase fashion around the dislocation axis. In the BP structure, this layer symmetry is broken and the layers escape along the dislocation axis. The CL solution has the narrowest core region since its structure is the most compatible with the topology of the smectic layers. The core structures differ remarkably in the Frank elastic nematic component: (i) the nematic twist contribution is dominant in DT, (ii) the bend distortion in CL, and (iii) all the nematic elastic distortions are involved in the BP structure. In the BP solution, the anisotropy of the elastic constants that are effective at the I/N interface also plays an important role. It is also to be stressed the $\vartheta - \vartheta_b$ dependence of all the solutions tends exponentially to zero with distance $\rho$ far from the dislocation axis, in accordance with results of Day *et al.* [11].

We have found that, for a sensible set of material constants, only the DT or CL solutions can be stabilized. In this respect, the coupling constant $D$ between the smectic and nematic order parameter is important. The coupling $D$ strongly affects the core region. With increased $D$, the DT and CL core structures, apart from the director field, become similar and the core size is decreased. Our calculations indicate that, in general, the DT solution is stable in the low $D$ regime, and the CL solution in the high $D$ regime.

We have in addition treated the case in which the liquid crystal is composed of a racemic mixture of conformers with competing chirality. We show that particularly the DT core structure significantly affects the spatial dependence $\Delta c(\rho)$ of conformer concentrations. A feedback effect of induced $\Delta c(\rho)$ variation on the nematic director field is negligible for conventional experimental conditions.

It is to be stressed that our approach is only qualitatively correct. A detailed quantitative study would require introduction of additional coupling terms between the nematic and smectic variational parameters. Indeed, comparison with existing [28] and ongoing [29] investigations of the smectic free energy structure based on a microscopic theory suggests that the coupling between nematic and smectic components is much more complex. However, we believe that these corrections would not affect the qualitative picture of our model. It is also to be mentioned that the gradient of the phase factor diverges as $\rho - > 0$ for all the solutions: $|\nabla\phi| = \sqrt{[1 + (M^2/\rho^2)]}$ for the DT and CL solutions and $|\nabla\phi| = \sqrt{[1 + (M^2/\rho^2 + (\partial u/\partial\rho)^2]}$ for the BP solution. Thus very close to the dislocation axis, $|\nabla\phi(\rho < 1)| \approx M/\rho$ for the first two solutions. Divergence of $|\nabla\phi|$ in this limit suggests that higher order gradient terms (for example $|\mathbf{n}\cdot\nabla - iq_0)^p\psi|^2$ with $p > 1$ [8]) should be included in the theory. However the solutions begin to differ significantly even at $\rho \gg 1$ (i.e. $\rho/\xi_\perp \approx 1$) with decreasing $\rho$ where $|\nabla\phi| \ll 1$. Therefore we expect that these higher order terms would not introduce qualitative changes or destabilize some of the solutions.

## Appendix A

*Euler–Lagrange equations*

The dimensionless free energy functional $g$ that we use to describe the core structure is given by equations (2), (4) and (8). Let us denote the variational parameters of our model by $v_i$, where $v_1 + \eta(\rho)$, $v_2 = u(\rho)$, $v_3 = s(\rho)$, $v_4 = \vartheta(\rho)$ and $v_5 = \alpha(\rho)$. In this notation

$$g = g\left[\left\{v_i, \frac{\partial v_i}{\partial\rho}\right\}\right].$$

The minimization of $g$ gives five coupled Euler–Lagrange differential equations

$$\frac{\partial g}{\partial v_i} - \frac{\partial}{\partial\rho}\frac{\partial g}{\partial\left(\frac{\partial v_i}{\partial\rho}\right)} = 0. \tag{A 1}$$

These are

$$(t - t_n)s - s^2 + s^3 - D\epsilon^2 + 2C_1 s H_N^{(1)} - 2C_1\frac{1}{\rho}\frac{\partial}{\partial\rho}\left(\rho H_N^{(2)}\frac{\partial s}{\partial\rho}\right) = 0, \tag{A 1 a}$$

$$C_2((rt - t_s)\epsilon + \epsilon^3 + \epsilon^5) - D\epsilon s + C_3\epsilon H_S^{(1)} - C_3\frac{1}{\rho}\frac{\partial}{\partial\rho}\left(\rho H_S^{(2)}\frac{\partial\epsilon}{\partial\rho}\right) = 0, \tag{A 1 b}$$

$$\frac{\partial}{\partial\rho}\left(\rho\epsilon^2\frac{\partial H_S^{(1)}}{\partial\left(\frac{\partial u}{\partial\rho}\right)}\right) = 0, \tag{A 1 c}$$

$$C_3\left(\epsilon^2\frac{\partial H_S^{(1)}}{\partial\vartheta} + \left(\frac{\partial\epsilon}{\partial\rho}\right)^2\frac{\partial H_S^{(2)}}{\partial\vartheta}\right) + C_1\left(s^2\frac{\partial H_N^{(1)}}{\partial\vartheta} + \left(\frac{\partial s}{\partial\rho}\right)^2\frac{\partial H_N^{(2)}}{\partial\vartheta}\right) - \frac{C_1}{\rho}\frac{\partial}{\partial\rho}\left(\rho s^2\frac{\partial H_N^{(1)}}{\partial\left(\frac{\partial\vartheta}{\partial\rho}\right)}\right) = 0, \tag{A 1 d}$$

$$C_3\left(\epsilon^2\frac{\partial H_S^{(1)}}{\partial\alpha}+\left(\frac{\partial\epsilon}{\partial\rho}\right)^2\frac{\partial H_S^{(2)}}{\partial\alpha}\right)+C_1\left(s^2\frac{\partial H_N^{(1)}}{\partial\alpha}+\left(\frac{\partial s}{\partial\rho}\right)^2\frac{\partial H_N^{(2)}}{\partial\alpha}\right)-\frac{C_1}{\rho}\frac{\partial}{\partial\rho}\left(\rho s^2\frac{\partial H_N^{(1)}}{\partial\left(\frac{\partial\alpha}{\partial\rho}\right)}\right)=0. \quad (A\,1e)$$

The quantities $H_N^{(1)}$, $H_N^{(2)}$, $H_S^{(1)}$, $H_S^{(2)}$ are defined in equations (8*c–f*).

It is also possible to examine analytically the limiting behaviours of these equations in the cases $\rho\to 0,\ \infty$. Because the equations are extremely complex, we consider the case of equal elastic constants, i.e.

$$a_i\equiv K_i/K_1=R\equiv\gamma_\perp/\gamma_\parallel=1,\ i=(\parallel,\perp,2,3).$$

In the approximation of equal elastic constant, equations (A1) simplify to

$$\frac{\partial^2 s}{\partial\rho^2}+\frac{1}{\rho}\frac{\partial s}{\partial\rho}-\frac{3}{C_1}((t-t_n)s-s^2+s^3-D\epsilon^2)-3s\left(\frac{\sin^2\vartheta}{\rho^2}+\frac{\partial\vartheta}{\partial\rho}\frac{\sin(2\vartheta)}{\rho}+\left(\frac{\partial\vartheta}{\partial\rho}\right)^2+\left(\frac{\partial\alpha}{\partial\rho}\right)^2\sin^2\vartheta\right)=0, \quad (A\,2a)$$

$$\frac{\partial^2\epsilon}{\partial\rho^2}+\frac{1}{\rho}\frac{\partial\epsilon}{\partial\rho}-\frac{C_2}{C_3}((rt-t_s)\epsilon+\epsilon^3+\epsilon^5)+\frac{D}{C_3}\epsilon s-\epsilon\left(\left(\frac{\partial u}{\partial\rho}\right)^2+\frac{M^2}{\rho^2}+2-2\left(\frac{\partial u}{\partial\rho}\sin\vartheta\cos\alpha+\frac{M}{\rho}\sin\vartheta\sin\alpha+\cos\vartheta\right)\right)=0, \quad (A\,2b)$$

$$\frac{\partial^2 u}{\partial\rho^2}+\frac{1}{\rho}\frac{\partial u}{\partial\rho}-\frac{\sin\vartheta\cos\alpha}{\rho}-\frac{\partial\vartheta}{\partial\rho}\cos\vartheta\cos\alpha+\frac{\partial\alpha}{\partial\rho}\sin\vartheta\sin\alpha+\frac{2\partial\epsilon}{\epsilon\partial\rho}\left(\frac{\partial u}{\partial\rho}-\sin\vartheta\cos\alpha\right)=0, \quad (A\,2c)$$

$$s^2\left(\frac{\sin(2\vartheta)}{2}\left(\frac{1}{\rho^2}+\left(\frac{\partial\alpha}{\partial\rho}\right)^2\right)-\frac{\partial^2\vartheta}{\partial\rho^2}+\frac{1}{\rho}\frac{\vartheta}{\partial\rho}\right)-s\frac{\partial s}{\partial\rho}\left(\frac{\sin(2\vartheta)}{\rho}+2\frac{\partial\vartheta}{\partial\rho}\right)+\frac{C_3}{C_1}2\epsilon^2\left(\frac{\partial u}{\partial\rho}\sin\vartheta\cos\alpha+\frac{M}{\rho}\cos\vartheta\sin\alpha-\sin\vartheta\right)=0, \quad (A\,2d)$$

$$\left(\frac{\partial^2\alpha}{\partial\rho^2}+\frac{1}{\rho}\frac{\partial\alpha}{\partial\rho}\right)\sin\vartheta+\frac{\partial\alpha}{\partial\rho}\frac{\partial\vartheta}{\partial\rho}2\cos(\vartheta)+2s\frac{\partial s}{\partial\rho}\frac{\partial\alpha}{\partial\rho}\sin\vartheta+\frac{C_3}{C_1}2\epsilon^2\left(\frac{M}{\rho}\cos\alpha-\frac{\partial u}{\partial\rho}\sin\alpha\right)=0. \quad (A\,2e)$$

In § 5 we introduce chirality into the model. This necessitates additional contributions to free energy, given by equations (16*a, b*), and an additional variational parameter $\Delta c(\rho)$.

The equation describing the dependence of $\Delta c(\rho)$ is

$$\Delta c(\rho)=\frac{\exp[\kappa(\rho)]-1}{\exp[\kappa(\rho)]+1}, \quad (A\,3)$$

where

$$\kappa(\rho)=\frac{2C_1 s^2 a_2\gamma_t}{C_4 t}H_t,$$

$$H_t=\mathbf{n}\cdot\nabla\times\mathbf{n}=\sin\alpha\left(\frac{\partial\vartheta}{\partial\rho}+\frac{\sin(2\vartheta)}{2\rho}\right)+\frac{\cos\alpha\sin(2\vartheta)}{2}\frac{\partial\alpha}{\partial\rho}.$$

The $\Delta c(\rho)$ variation changes equations (A 1 *a, d, e*). Equation (A1 *a*) modifies into

$$(t-t_n)s-s^2+s^3-D\epsilon^2+2C_1 sH_N^{(1)}-2C_1\frac{1}{\rho}\frac{\partial}{\partial\rho}\left(\rho H_N^{(2)}\frac{\partial s}{\partial\rho}\right)-2C_1 a_2\gamma_t s\Delta c H_t=0,$$

equation (A1 *d*) into

$$C_3\left(\epsilon^2\frac{\partial H_S^{(1)}}{\partial\vartheta}+\left(\frac{\partial\epsilon}{\partial\rho}\right)^2\frac{\partial H_S^{(2)}}{\partial\vartheta}\right)+C_1\left(s^2\frac{\partial H_N^{(1)}}{\partial\vartheta}+\left(\frac{\partial s}{\partial\rho}\right)^2\frac{\partial H_N^{(2)}}{\partial\vartheta}\right)-\frac{C_1}{\rho}\frac{\partial}{\partial\rho}\left(\rho s^2\frac{\partial H_N^{(1)}}{\partial\left(\frac{\partial\vartheta}{\partial\rho}\right)}\right)-C_1 a_2\gamma_t s^2\Delta c\frac{\partial H_t}{\partial\vartheta}+C_1 a_2\gamma_t\frac{1}{\rho}\frac{\partial}{\partial\rho}\left(\rho s^2\Delta c\frac{\partial H_t}{\partial\left(\frac{\partial\vartheta}{\partial\rho}\right)}\right)=0,$$

and equation (A1 *e*) into

$$C_3\left(\epsilon^2\frac{\partial H_S^{(1)}}{\partial\alpha}+\left(\frac{\partial\epsilon}{\partial\rho}\right)^2\frac{\partial H_S^{(2)}}{\partial\alpha}\right)+C_1\left(s^2\frac{\partial H_N^{(1)}}{\partial\alpha}+\left(\frac{\partial s}{\partial\rho}\right)^2\frac{\partial H_N^{(2)}}{\partial\alpha}\right)-\frac{C_1}{\rho}\frac{\partial}{\partial\rho}\left(\rho s^2\frac{\partial H_N^{(1)}}{\partial\left(\frac{\partial\alpha}{\partial\rho}\right)}\right)-C_1 a_2\gamma_t s^2\Delta c\frac{\partial H_t}{\partial\alpha}+C_1 a_2\gamma_t\frac{1}{\rho}\frac{\partial}{\partial\rho}\left(\rho s^2\Delta c\frac{\partial H_t}{\partial\left(\frac{\partial\alpha}{\partial\rho}\right)}\right)=0.$$

The equations are solved using the relaxation method [23]. In our numerical calculations, because of the strong variation of the parameters $v_i$ close to the dislocation axis, we use the transformation $x = \ln(\rho/L)$, where $L$ describes the size of the box used in the calculations. We set $L = 150$, where departures of variational parameters from their bulk values are already negligible.

## Appendix B

*Choice of material constants*

The reference set values of the dimensionless constants of our model are given in § 3.2. Here we discuss the criteria for these choices.

The nematic component material constants which occur in equations (1 $a, b$), in 5CB take the values [30]: $a_0 \sim 40 \times 10^6\,\mathrm{J\,m^{-3}}$, $b \sim 2 \times 10^6\,\mathrm{J\,m^{-3}}$, $c \sim 4 \times 10^6\,\mathrm{J\,m^{-3}}$, $k_i \sim 10^{-11}\,\mathrm{J\,m^{-1}}$ $(i = 1, 2, 3)$, $T^*_{\mathrm{NI}} \sim 307°\mathrm{K}$. These values are typical of a wide class of liquid crystals. For the smectic material constants, defined in equations (1 $c, d$), we set similar values: $\alpha_0 \approx a_0$, $\beta \approx b$, $\gamma \approx c$, $\gamma_\parallel \approx \gamma_\perp \approx k_i$. We chose as a sensible value for our calculations, at $D = 0$, $T^*_{\mathrm{NI}} - T^*_{\mathrm{SN}} = 10°\mathrm{K}$. This choice suggests: $a_2 \sim a_3 \sim a_\parallel \sim a_\perp \sim R \sim 1$, $C_1 \sim C_3 \sim 100$, $C_2 \sim 1$, $t_n \sim t_S \sim 50$, $r \sim 1{\cdot}03$. The reference set, shown in § 3.2, is set slightly away of the values just listed in order to get closer to the regime where the CL and BP structures can exist.

S.K. gratefully acknowledges the financial support of the Slovenian Ministry of Science and Technology and the Open Society Fund of Slovenia. We thank T. C. Lubensky, J. Prost and J. W. Goodby for useful conversations.



## References

[1] Mermin, N. D., 1976, *Rev. mod. Phys.*, **51,** 591.
[2] Kléman, M., 1983, *Points, Lines and Walls* (John Wiley, Chichester), Chap. 6.
[3] Lyusyuktov, I. F., 1979, *Soviet Phys. JETP*, **48,** 178.
[4] de Gennes, P. G., 1974, *The Physics of Liquid Crystals* (Oxford University Press).
[5] de Gennes, P. G., 1972, *Solid St. Commun.*, **10,** 753.
[6] Tinkham, M., 1975, *Introduction to Superconductivity* (McGraw-Hill).
[7] Renn, S. R., and Lubensky, T. C., 1988, *Phys. Rev.* A, **38,** 2132.
[8] Lubensky, T. C., and Renn, S. R., 1990, *Phys. Rev.* A, **42,** 4392.
[9] Lavrentovich, O. D., Nastishin, Yu. A., Kulishov, V. I., Narkevich, Yu. S., Tolochko, A. S., and Shiyanovskii, S. V., 1980, *Europhys. Lett.*, **13,** 313.
[10] Goodby, J. W., Waugh, M. A., Stein, S. M., Chin, E., Pindak, R., and Patel, J. S., 1989, *Nature, Lond.*, **337,** 449.
[11] Day, A. R., Lubensky, T. C., and McKane, A. J., 1983, *Phys. Rev.* A, **27,** 1461.
[12] Loginov, E. B., and Terentjev, E. M., 1987, *Soviet Phys. Crystallogr.*, **32,** 166.
[13] Kléman, M., 1974, *J. Phys. Paris*, **35,** 595.
[14] Kralj, S., and Sluckin, T. J., 1993, *Phys. Rev.* E, **48,** 3244.
[15] Schopohl, N., and Sluckin, T. J., 1987, *Phys. Rev. Lett.*, **59,** 2582. Note that a comprehensive discussion of defect structure in nematic liquid crystals requires consideration of local biaxiality.
[16] Poniewierski, A., and Sluckin, T. J., 1985, *Molec. Phys.*, **55,** 1113.
[17] Kralj, S., and Žumer, S., 1992, *Phys. Rev.* A, **45,** 2461.
[18] Thoen, J., Marynissen, H., and van Dael, W., 1984, *Phys. Rev. Lett.*, **52,** 204.
[19] Lubensky, T. C., 1983, *J. Chim. phys.*, **80,** 31.
[20] See for example, McMillan, W. L., 1971, *Phys. Rev.* A, **4,** 1238.
[21] Rosenblatt, C., and Ronis, D., 1981, *Phys. Rev.* A, **23,** 305.
[22] Pawlowska, Z., Kventsel, G. F., and Sluckin, T. J., 1988, *Phys. rev.* A, **38,** 5342.
[23] Press, W. H., Flannery, B. P., Teukolsky, S. A., and Vetterling, W. T., 1986, *Numerical Recipes* (Cambridge University Pres).
[24] Leslie, F. M., Stewart, I. W., Carlsson, T., and Nakagawa, M., 1991, *Cont. Mech. Thermodyn.*, **3,** 237.
[25] Trebin, H. R., 1982, *Adv. Phys.*, **31,** 195.
[26] Press, M. J., and Arrott, A. S., 1975, *J. Phys. Paris*, **36,** C1–177.
[27] Williams, R. D., 1986, *J. Phys.* A, **19,** 3211.
[28] Linhananta, A., and Sullivan, D. E., 1991, *Phys. Rev.* A, **44,** 8189.
[29] Velasco, E., and Sluckin, T. J. (in preparation).
[30] Sheng, P., 1982, *Phys. Rev.* A, **3,** 1610.